Non-contact full field vibration measurement based on phase-shifting

Hiroyuki Kayaba
Nikon Corporation, Japan
Hiroyuki.Kayaba@nikon.com

Yuji Kokumai
Nikon Corporation, Japan
Yuji.Kokumai@nikon.com

Abstract

Vibration measurement systems are widely used in the industry. A variety of vibration measurement techniques are proposed, including methods using an acceleration sensor, a laser displacement meter, and tracking a marker with a camera. However, these methods have limitations that allow only one point to be measured and require markers. We present a novel, non-contact full field joint measurement technique both of vibrations and shape based on phase-shifting. Our key idea is to acquire the frequency of vibrating objects using FFT to analyze the phase-shift error of vibrating objects. Our proposed algorithm estimates the phase-shift error by iterating frame-to-frame optimization and pixel-to-pixel optimization. A feature of our approach is to measure the surface of vibration at different frequencies without markers or texture in full fields. Our developed system is a low cost system, which is composed of a digital-light-processing (DLP) projector and camera (100 frames per second). The results of our experiments show that low frequency vibration of objects can be measured in a non-contact manner with high accuracy. Also, reconstruction of the vibrating object surface can be performed with high accuracy.

1. Introduction

Measurement of 3D shapes is quite important in many fields ranging from manufacturing to medicine [3]. This technique is widely used in fields such as computer vision, robot navigation, computer graphics, and preservation of heritage [22]. Therefore, numerous techniques have been developed so far to acquire the 3D shape of an object. The phase-shifting technique has been studied and widely used in many fields due to its high accuracy. Furthermore, a 3D measurement technique for estimating vibration has been proposed. In recent years, there is a growing demand for measurement of vibrating objects in industrial and research fields. For instance, vibration measurement is used to check for part defects, perform building maintenance, and observe the effect of vibration on targets such as a vibrating car engine. A variety of vibration measurement techniques based on a laser displacement meter and image processing such as marker tracking or optical flow have been developed. However, the typical vibration measurement systems require that many markers be placed on the objects and also require a rich texture object. These techniques require use of a high resolution, high speed camera. Moreover, a laser displacement meter has further drawbacks in that it cannot measure the entire surface of an object at the same time. These sensors usually measures one point on the surface of an object. Therefore, we developed a novel, non-contact full field vibration measurement method for a vibrating object surface without the need for markers or rich textures.

Our key idea is to estimate the frequency of a vibrating object by analyzing the phase-shift error. Our proposed algorithm estimates the phase-shift error from iterative optimization, on a pixel-to-pixel basis and on frame-to-frame basis. In pixel-to-pixel optimization, the variables which represent the DC component of the sinusoidal fringe pattern, amplitude component, and initial phase are estimated. In frame-to-frame optimization, the variables which represent phase-shifting offset are estimated. The technique to solve this problem was developed by assuming constant acceleration motion for the movement of vibrating objects [23]. However, the above technique cannot deal with vibration for movement with non-constant velocity. In general, the movement of vibrating objects usually includes translation and rotation motion. This movement is nonlinear movement. Therefore, we have developed a method that corrects phase-shift errors using iterative optimization. Also, the frequency of a vibrating object is measured by analyzing the estimated phase-shift error during measurement. Our measurement system is composed of a DLP projector and a synchronized camera. This system can measure low frequency vibration of objects. Our system's limitation is based on the sampling theorem since a sinusoidal pattern for calculating phase is projected. The detectable frequency of our system is limited by the camera frame rate.

This paper is organized as follows. Section 2 describes re-

lated work. Section 3 explains least squares phase-shifting algorithms. Section 4 proposes that our proposed method can correct phase-shift errors using iterative optimization. Section 5 shows the effectiveness of the proposed method in simulation data. Section 6 shows the experiment results. Section 7 discusses limitations. Section 8 discusses conclusion and future works.

2. Related Work

Vibration measurement: A variety of non-contact vibration measurement techniques are proposed, including methods of measuring an object with an acceleration sensor, using a laser displacement meter, and tracking a marker with a camera. The laser Doppler vibrometer has also been used for civil applications [20]. Also, extraction of speech sources from the movement of a speckle pattern laser projected onto vibrating objects has been proposed [25]. Among the above methods, the laser vibration measurement method can only measure one point which is irradiated by a laser. Moreover, these methods cannot measure the entire surface of an object at the same time.
Another approach is vibration measurement based on computer vision techniques. The method tracks planar targets mounted on a vibrating structure in a sequence of captured images [14]. This method is a way of responding to multi-point displacement using image processing techniques [16]. This method analyzes an image sequence of vibrating objects using the optical flow [15]. This method amplifies subtle invisible motion in video scenes [17] [24]. However, the accuracy of this approach, which is based on image processing, depends highly on the scene. This approach requires the object to have rich textures. A method that is very similar to our proposed method is to measure vibration using a z-displacement which is measured at high speed and with high accuracy [27]. The difference between this method and our approach is that this method requires an expensive high speed camera and projection system whereas our setup consists of low cost equipment.

Phase-shifting: Over the past decades, numerous techniques have been proposed to acquire the 3D shape of an object utilizing different principles [6]. These methods include time of flight, laser triangulation, structured from motion, and stereo vision. Among them, stereo vision is widely used and is divided into active stereo and passive stereo. Phase-shifting is an active stereo method. The principle of phase-shifting is to calculate three-dimensional coordinate values from the phase value, which is obtained by shifting the phase of a projected pattern using a triangulation method. As a feature of phase-shifting, this method can measure objects with poor texture with high accuracy and high resolution. Numerous phase-shifting techniques have been developed. One method is high speed measurement using color fringes in RGB space [13] [28]. This method adaptively sets the camera exposure time for capturing HDR images [4]. This method performs measurement in real time with high precision using a DLP projector [12] [26]. Moreover, an LED-based multi-aperture projection system [11] is faster than other traditional methods. In addition, a technique for the phase-shift error analysis is proposed [1]. The development of these phase-shifting techniques has been classified [8].

3. Least Squares Phase-Shifting Algorithm

Phase-shifting algorithms are widely used in optical metrology due to their speed and accuracy [18]. The principle of this algorithm is to periodically project a pattern on an object while shifting an arbitrarily phase offset. Over the years, numerous phase-shifting algorithms, including three steps, four steps, or more, have been developed. The number of phase-shifting images is typically between three and sixteen. In general, as the number of images used increases, higher quality accuracy is expected but the calculation cost rises. In this paper, a six step phase-shifting algorithm with a phase-shifting of $\pi/3$ is used to balance accuracy and speed. A phase-shifting offset ϕ_n is expressed by eq.(1),

$$\phi_n = \frac{2\pi n}{N} \tag{1}$$

where N is the number of sinusoidal patterns and n is the phase shift step number. Note that (x, y) are the pixel coordinates in the captured images and I_n is the intensity at point (x, y).

$$I_n(x, y) = B(x, y) + A(x, y)\cos(\phi(x, y) + \phi_n) \tag{2}$$

where $A(x, y)$ is the intensity modulation, $B(x, y)$ is the average intensity, and $\phi(x, y)$ is the phase which is unknown variables. A least squares phase-shifting algorithm is implemented in our vibration measurement system. Solving eq.(3) using the least-squares algorithm, we obtain $\phi(x, y)$ as follows:

$$\phi(x, y) = tan^{-1}\left(\frac{-\sum_{n=1}^{N} I_n \sin(\phi_n)}{\sum_{n=1}^{N} I_n \cos(\phi_n)}\right). \tag{3}$$

This equation provides the wrapped phase ranging from $[-\pi, \pi)$. A temporal phase unwrapping algorithm is used for removing 2π discontinuities. This phase can be converted to a 3D shape when the system is calibrated. A variety of phase-unwrapping algorithms have been proposed so far such as algorithms devising an integrated sequence [7], using a binary code [9], using a Gray code [21], and using a periodic pattern of a plurality of wavelengths [29] [2]. As a robust method for ambient light, there is a method using XOR code [10]. Furthermore, a method which does not require unwrapping has been proposed [19].

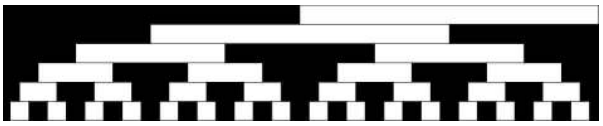

Figure 1. Conventional Gray codes pattern.

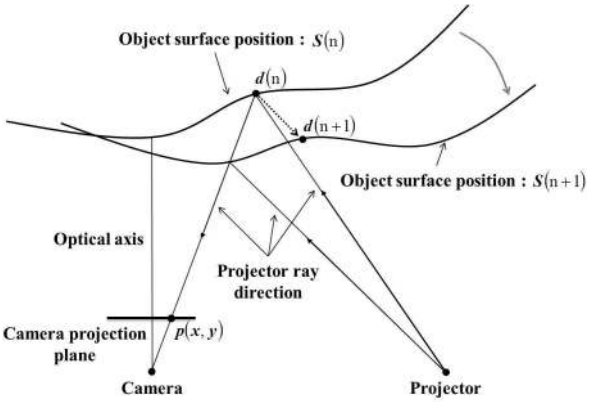

Figure 2. Phase-shift errors caused by object or projector movement during measurement. These errors are usually non-linear.

In this paper, the phase-unwrapping algorithm with Gray codes is used. Gray codes which are well known for easy to implement is shown in Figure 1. The width of one cycle sinusoidal is strongly related to the amplitude of detectable vibrating objects. The detection of vibration is quite hard if the amplitude is larger than this width. This width was set experimentally. The relationship between the wrapped phase and the unwrapped phase can be written as:

$$\phi'(x,y) = \phi(x,y) + k(x,y) \times 2\pi, \quad k(x,y) \in [0, M-1]. \tag{4}$$

Let $\phi'(x,y)$, $k(x,y)$, and M be the unwrapped phase, an integer number, and the number of phases from the projector, respectively. $\phi'(x,y)$ is determined from eq.(4). Once the continuous phase map is obtained, the phase at each pixel can be converted to a depth map when the system is calibrated. Then, 3D results are obtained from $\phi'(x,y)$ using this system based on triangulation. Measurement speed is limited by the frame rate of the camera and projector. In this paper, the measurement data is processed off-line and the vibration measurement speed is up to 100 Hz.

4. Non-linear Correction of Phase Error

In typical phase-shifting techniques, measurement of a correct phase-shifting offset is quite difficult when the relationship between the objects and the projector projection are changed during projection of the sinusoidal patterns from a projector. Figure 2 shows a vibrating object projecting the sinusoidal patterns from a projector. Let $p(x,y)$, n, $S(n)$, and $d(n)$ be the camera pixel, the number of images, the object surface, and the point onto $S(n)$, respectively. Now that $S(n)$ and $d(n)$ move to $S(n+1)$ and $d(n+1)$ while the object is vibrating. Therefore, $d(n+1)$ is not captured at $p(x,y)$ in the (n+1)th image due to change in the relative position between the measurement system and the object. The correct sinusoidal patterns with phase-shifting offset are not observed when the object position is changed in images. The amount of the phase-shift error is large when there is a large amount of object movement.

Thus, we developed a novel vibration measurement system using analysis of the phase-shift offset error of the vibrating object. This system robustly measures the frequency of a vibrating object. Also, high accuracy 3D reconstruction of vibrating objects was attained in order to compensate for the phase-shift offset error. Our proposed method can estimate the phase-shift offset error using pixel-to-pixel optimization of each unknown pixel variable (see Section 4.1) and frame-to-frame optimization for each image variable (see Section 4.2). Eq.(2) can be expanded as follows:

$$\begin{aligned} I_n(x,y) &= B(x,y) + A(x,y)\cos(\phi(x,y) + \phi_n) \\ &= B(x,y) + A(x,y)\cos\phi(x,y)\cos\phi_n \\ &\quad - A(x,y)\sin\phi(x,y)\sin\phi_n. \end{aligned} \tag{5}$$

If we define $p(x,y)$, $q(x,y)$, $r(x,y)$, s_n and t_n by

$$\begin{aligned} p(x,y) &= B(x,y) \\ q(x,y) &= A(x,y)\cos\phi(x,y) \\ r(x,y) &= -A(x,y)\sin\phi(x,y) \\ s_n &= \cos\phi_n \\ t_n &= \sin\phi_n. \end{aligned} \tag{6}$$

Eq.(5) can also be rewritten as follow:

$$I_n(x,y) = p(x,y) + q(x,y)s_n + r(x,y)t_n \tag{7}$$

where $p(x,y)$, $q(x,y)$ and $r(x,y)$ are an unknown variables at each pixel. s_n and t_n are optimized at each image. When the objects is vibrating, s_n and t_n are changing. The phase-shift offset error, which is caused by vibration, is assumed to be constant in the ROI (region of interest) image. If the number of sinusoidal images is insufficient, estimation of highly reliable variables may not be possible. Since the solution to the variables is not sufficiently converged. Hence, we solve eq.(7) by using iterative optimization. The estimated phase-shifting offset $\hat{\phi}_n(x,y)$ is obtained from the optimized $I_n(x,y)$. The phase residual is then defined as

$$\Delta\phi_n(x,y) = \hat{\phi}_n(x,y) - \phi_n \tag{8}$$

where $\Delta\phi_n(x,y)$ is the phase error residual. The system can measure the frequency of the objects using FFT analysis

of $\Delta\phi_n(x, y)$ and correct the non-linear phase-shift offset error with high accuracy. Our system can reconstruct a 3D shape of the non-linearly vibrating objects. Note that it is hard to measure the objects which are vibrating with more than the period of a sinusoidal. Therefore, it is desirable for the period length of the sinusoidal pattern to be changed depending on the object.

4.1. Pixel-to-pixel optimization

This subsection describes the optimization of common variables at each pixel. We assumed two conditions. First, an point of interest of an object is captured at the same pixel in the images. Second, the reflection intensity and the ambient light on the object surface are not changed during measurement. When s_i and t_i are fixed, eq.(9) is described as

$$\begin{bmatrix} 1 & s_1 & t_1 \\ \vdots & \vdots & \vdots \\ 1 & s_n & t_n \end{bmatrix} \begin{bmatrix} p(x,y) \\ q(x,y) \\ r(x,y) \end{bmatrix} = \begin{bmatrix} I_1(x,y) \\ \vdots \\ I_n(x,y) \end{bmatrix} \tag{9}$$

where p_i, q_i, and r_i are wrapped phase, DC component and AC component of intensity, respectively. Assume that these variables are constant at each pixel from eq.(9). The variables $p(x, y)$, $q(x, y)$, and $r(x, y)$ are solved using the least squares method.

4.2. Frame-to-frame optimization

This subsection describes the optimization of common variables in an image. The variables s_i and t_i, which are the phase shifted value of each image, are assumed to be constant in the ROI image window. When p_i, q_i and r_i are fixed, eq.(10) is describes as

$$\begin{bmatrix} q_1 & r_1 \\ \vdots & \vdots \\ q_l & r_l \end{bmatrix} \begin{bmatrix} s_n \\ t_n \end{bmatrix} = \begin{bmatrix} I_1 - p_1 \\ \vdots \\ I_l - p_n \end{bmatrix} \tag{10}$$

where l is the number of pixels in the ROI image. Besides, the following relationship is established between s_n and t_n.

$$(s_n)^2 + (t_n)^2 = 1. \tag{11}$$

As we see, s_i and t_i are solved using the least squares method under the restraint condition of eq.(11). It is assumed that a vibrating object and a stable object are not in the window at the same time. The window size is defined so that it includes at least one period of a sinusoidal pattern. This size is a trade-off between calculation time and the stability of solutions. In our experiments, this size was set to an oblong rectangle since the projected sinusoidal patterns have a small amount of change to the horizontal axis direction and is experimentally defined by the camera pixels and the object size. Also, this size is experimentally defined by the camera pixels and the object size.

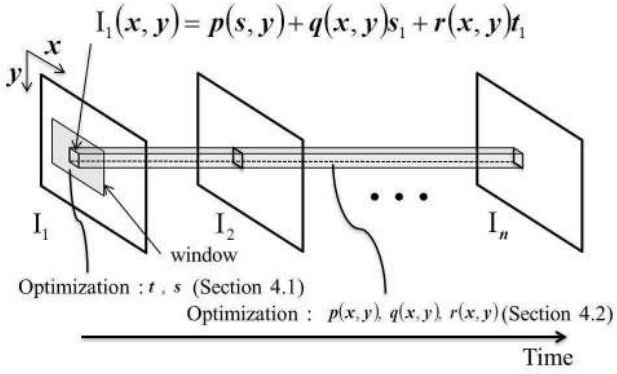

Figure 3. Iterative optimization performed frame-to-frame in the ROI image and optimization performed pixel-to-pixel in images.

Algorithm Non-contact full field vibration measurement based on phase-shifting

1. Project sinusoidal patterns and Gray codes. Phase-shift offset ϕ_n is $2\pi n/N$. Initialize s_n and t_n. The wrapped phase is obtained from the captured sinusoidal images. (Section 3)

2. Update each pixel of $p(x, y)$, $q(x, y)$, and $r(x, y)$ after optimization performed frame-to-frame when s_n and t_n are fixed. (Section 4.1)

3. Update each s_n and t_n in the ROI window after optimization performed pixel-to-pixel when $p(x, y)$, $q(x, y)$, and $r(x, y)$ are fixed. (Section 4.2)

4. Calculate the residual error $E_n(x, y)$ after iterative optimization. Repeat steps 2 and 3 until the convergence judgment has been satisfied. (Section 4.3)

5. Finish iterative optimization (steps 2 to 4). Calculate the estimated phase-shift error $\Delta\phi_n(x, y)$. Perform FFT analysis of the frequency of a vibrating object. (Section 4)

6. Calculate unwrapped phases using Gray codes. Reconstructed 3D shape is obtained from the unwrapped phase. (Section 4)

4.3. Phase-shift optimization

This subsection describes the optimization procedure for the phase-shift error offset. This procedure is shown in Figure 3. Optimization is iterated pixel-to-pixel (Section 4.1) and frame-to-frame (Section 4.2) until the threshold value for estimating unknown variables is satisfied. The **algorithm** shows the optimization procedure. The residual error

in each image is E_n. The average error in images is E_k. E_n and E_k are denoted by

$$E_n = \frac{1}{H \times W} \sum_{x=1}^{H} \sum_{y=1}^{W} (I_n(x,y) - I'_n(x,y))^2$$

$$E_k = \frac{1}{N} \sum_{n=1}^{N} E_n \tag{12}$$

where, $I'_n(x,y)$ is the intensity after optimization and k is the iteration number. Let W and H be the width and height of an image, respectively. The convergence judgments are as follows:

1. $E_k < T_E$
2. $k > K_{max}$
3. E_k - $E_{k-1} < T_K$

where, T_E is the threshold of the residual error, K_{max} is the maximum iteration number, and T_K is the threshold of the residual error between iterations. Each threshold is experimentally determined. After the optimization, vibration frequency can be measured by analyzing the phase-shift error.

5. Simulation Results

To investigate the performance of the proposed techniques, experimental simulation data was created. In this simulation, an object is assumed to be vibrating (f Hz) and is captured by a camera at intervals of t msec. Then, the phase-shift error is estimated at the pixel of interest and the frequency of vibration f is calculated using FFT analysis of the estimated phase-shift error. The phase-shift error at each pixel which is generated by the vibration is denoted by eq.(13)

$$e_n^1 = \alpha \, cos(2\pi f n t) \tag{13}$$

where α is modulation and n is the sampling number. This simulation data includes Gaussian noise with a zero mean and a variance σ^2 of 0.05. Gaussian noise $\mathcal{N}(0, \sigma^2)$ is denoted as e_n^2. The intensity $I_n(x,y)$ is denoted by eq.(14)

$$\begin{aligned} I_n(x,y) = B(x,y) + e_n^2 \\ + A(x,y)\cos(\phi(x,y) + \phi_n + e_n^1) \end{aligned} \tag{14}$$

In our experiment, three frequencies f were measured: 10, 20, and 50 Hz. We set each parameter n to 150, N to 3, and t to 10 msec. B(x, y) and A(x, y) are 0.5 in the constants. Figures 4 (a) and (b) show the results comparison of the true value and e_n^1 when f is 10 Hz. The result shows that the Root Means Square (RMS) error is 0.032. Figure 5 shows the results of FFT analysis of e_n^1. This frequency was analyzed using the FFTW library [5]. This results show that the proposed method can estimate the phase-shift error including Gaussian noise with high accuracy. Therefore, the frequency of vibrating objects can be estimated by analyzing the phase-shift error.

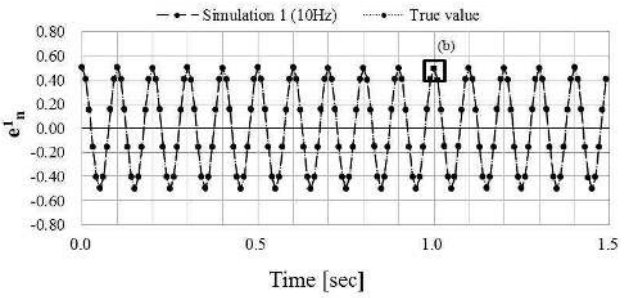

(a)

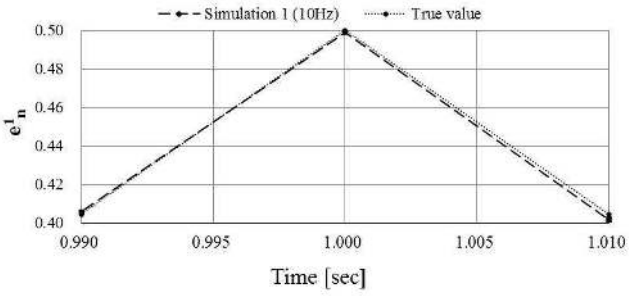

(b)

Figure 4. Results of phase-shift error estimation in simulation data (frequency of vibration: 10 Hz): (a) Comparison of estimated phase-shift $e_1(t)$ and true value and (b) Enlarged view of part of Figure 4 (a).

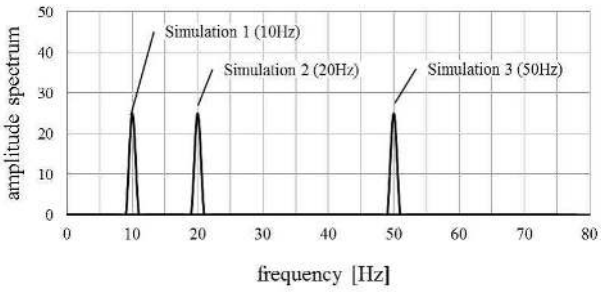

Figure 5. FFT spectrum analysis of simulation data results (frequency of vibration: f = 10, 20, and 50 Hz)

6. Experiments

6.1. Hardware system setup

Figure 6 shows our developed hardware system to measure vibrating objects. The system includes a DLP projector (Texas instruments. DLP Light crafter 4500) and a CMOS camera (Point Grey Research, Inc. FL3-U3-13S2M-CS). The camera is attached with a 3.8-13 mm focal length

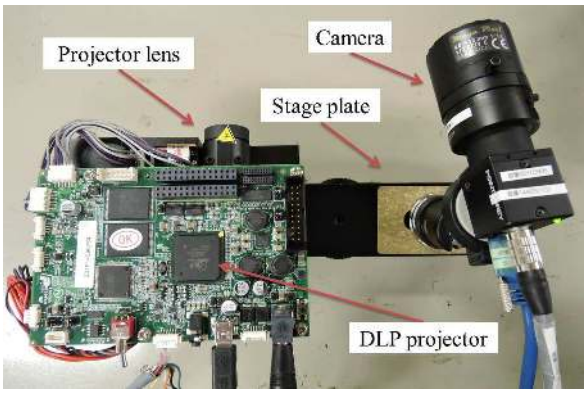

Figure 6. Experiment setup (our systems sensor)

Mega-pixel lens (FUJIFILM DA3.4×3.8SA-1) with F/1.4 to 16C and has a maximum frame rate of 120 frame/sec. The camera pixel size is 3.6 x 3.4 μm. The projector resolution and the camera resolution are 1140 x 912 and 1328 x 1048. This projector has an LED which produces approximately 150 lumen and has a 100 Hz refresh rate (8-bit sinusoidal patterns). Our system's frame rate t is 10 msec. The length of the sensor baseline (camera-projector distance) is 200 mm.

Our system's field of view is 300 mm (H) x 450 mm (W) when the camera-object distance is 500 mm. A non-contact laser displacement meter (KEYENCE IL-600) was used to measure a true value of the frequency of vibrating objects. The sensor accuracy in the z-axis direction is 50 μm. It was confirmed that our methods can measure the frequency of a vibrating object with high accuracy by comparing the experiment results and the true value obtained from a laser sensor. The ROI window size is experimentally set to 4 by 14 pixels (height by width) which is based on one stripe length in a phase image. For the iteration parameters, T_E is set to 0.01, K_{MAX} is set to 100, and T_K is set to 10^{-10}.

6.2. Experiment 1 : Vibrator

The sinusoidal vibration of objects generated by a vibrator was measured in this experiment. Figure 7 shows this vibrator and the vibration direction. The iron plate fixed on the vibrator was only vibrating toward the camera in this scene. The true value of the frequency of vibrating objects was obtained from the laser displacement meter. Figure 8 shows the z-axis displacement of the vibrator obtained from this laser sensor. The image number N is 100. The true frequency of the vibration objects obtained from FFT analysis of this result is 9.5 Hz.

Figure 9 shows the results of the vibration measurement in the experiment. This error occurs from only part of the vibrating iron plate. Figure 10 shows the relationship between the estimated phase-shift error at the pixel of interest on the

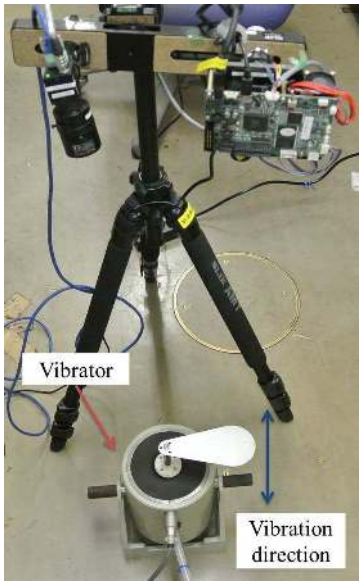

Figure 7. Setup of experiment 1 (vibrator)

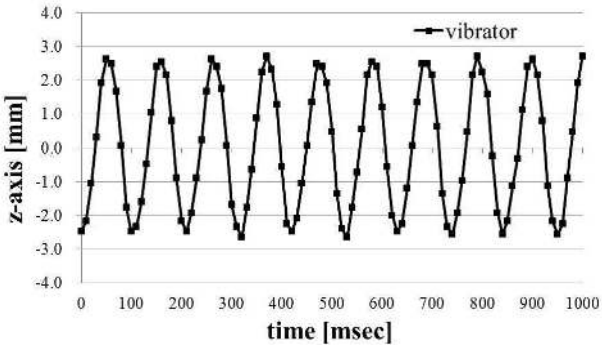

Figure 8. The vibration direction displacement (z-axis) of the vibrating objects.

vibrating surface and the sampling time. These results show that our proposed method can estimate the phase-shift error with high accuracy. The frequency of the pixel which is obtained from FFT analysis is 9.0 Hz. Figure 11 shows the results of vibration analysis. The estimated frequency error is 0.5 Hz when comparing the true value with the estimated result. Figure 12 shows the visualization results of the estimated frequency of all pixels. We call this a frequency map. The result of this experiment shows that our proposed method can measure low frequency of vibrating objects and that the measurement accuracy is 0.5 Hz.

6.3. Experiment 2 : Human motion

The frequency of a moving human hand and human breath were measured in this experiment. Then, the 3D shape of the moving human hand was reconstructed. Figure 13 shows the experiment results of vibration measurements. In this experiments, the hand was moving repeatedly from

(a) (b) (c) (d) (e)

Figure 9. Measurement results of vibrator displacement of vibratory equipment (frequency of vibration： 10 Hz): a) Original image of the object; b) Captured fringe image; c) to e) Phase-shift error images (color bar range from blue (-0.005) to red (0.005) t = 0 msec in c), 30 msec in d), and 60 msec in e))

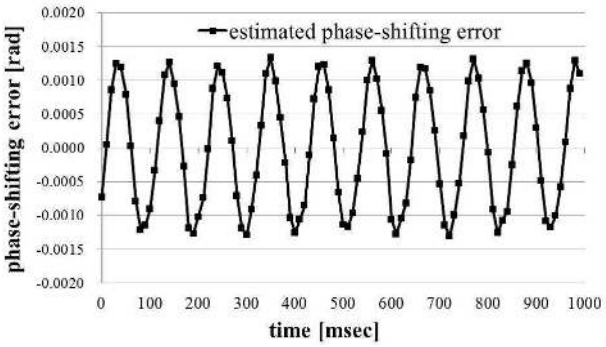

Figure 10. Cross section of the estimated phase-shift errors at a point of interest (frequency of vibration： 10 Hz)

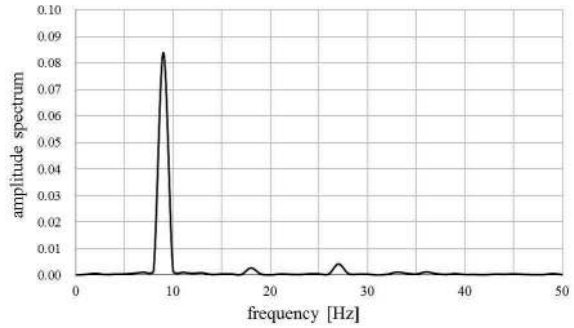

Figure 11. FFT analysis results at a point of interest on the vibrating surface

background to foreground and a person was breathing during the measurement. However, the estimated frequency of fingertips is of poor quality because the ROI image includes a foreground (human finger) and a background (wall) in frame-to-frame optimization. The phase-shift offset is different from the foreground and the background. Figure 14 shows the visualization results of the estimated frequency of all pixels. The frequency of the object is around 1.0-3.0 Hz. The abdomen was vibrating at 2.0-3.0 Hz. Figure 15 shows the 3D reconstruction result of the object. These results prove that our proposed system can measure the frequency of a non-linear vibrating object and reconstruct a 3D shape such as a human hand and human breath.

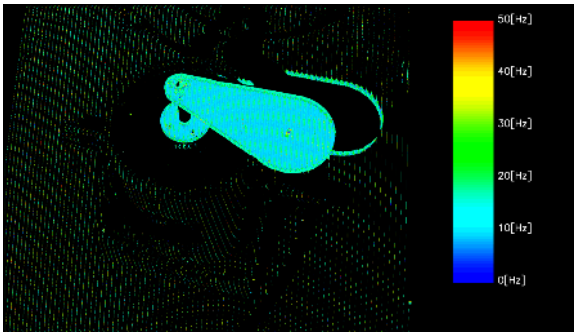

Figure 12. Frequency map of the vibrating iron plate (frequency of vibration：10 Hz).

7. Limitations

The detectable range of amplitude for vibrating objects is limited by the sinusoidal period of the projected pattern and lens blur. When a magnitude of vibration movement exceeds the sinusoidal period in the image and the depth of field of a lens is shallow, measurement accuracy deteriorates. Measurement accuracy also deteriorates when the foreground and background are captured in a ROI window at the same time. This effect gives greater edge portion.

The detectable range of the vibration frequency is limited by camera and projector speed. To measure objects vibrating at a high frequency, a high speed camera and a projector should be used. In other methods, binary codes can be used for high speed measurement; however, measurement accuracy deteriorates.

8. Conclusion

This paper has presented a novel non-contact full field vibration measurement system that measures errors in phase shifting. Our system is the same as that used for measuring a 3D shape using phase-shifting based structured light triangulation and consists of a low cost DLP projector and camera. The main idea is to take phase shifting-based structured light systems and derive a relationship between vibration of an object and errors in the predicted phase shift value. The

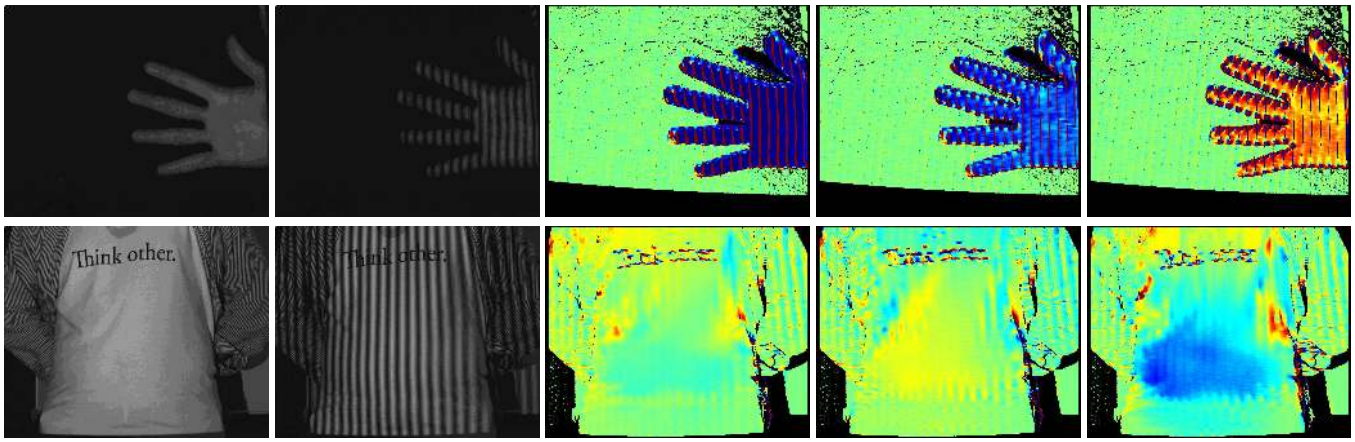

(a) (b) (c) (d) (e)

Figure 13. Vibration measurement results for a human hand (top) and human breathing (bottom): a) Original image of the object; b) Captured fringe image; c) to e) Phase-shift error images (color bar range from blue (-0.005) to red (0.005)) t = 0 msec in c), 300 msec in d), and 600 msec in e))

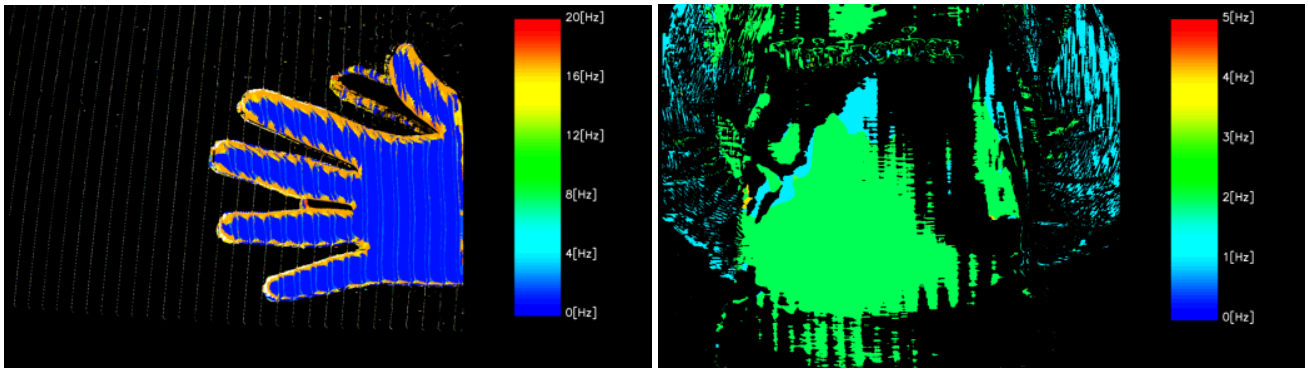

Figure 14. Frequency map of a moving human hand (Left) and human breath (Right) (frequency of vibration: 1.0-3.0 Hz).

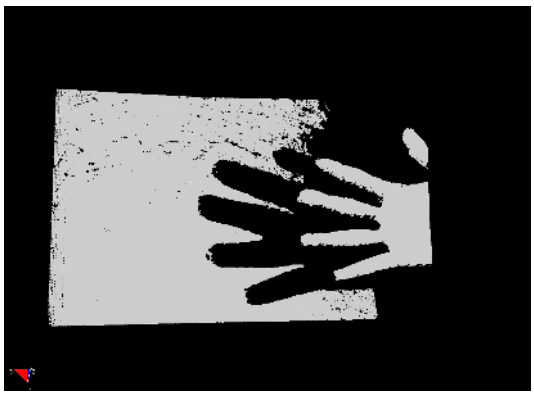

Figure 15. 3D reconstruction of a moving human hand. Foreground is a human hand and a background is a wall.

simulation and experiment results have proved that our system can perform high accuracy vibration measurement and reconstruct a 3D shape. Thus, we conclude that our system can measure movement of a vibrating object surface from captured images without markers and textures in a full field of view. The measurement range for the frequency of vibrating objects is 0-10 Hz with our system. These results have also proved that our system can measure a free moving vibrating object, such as a human hand and human breath.

In future work, improvements to measurement accuracy and measurement of high frequency vibrating objects using a high speed projector and camera will be made. Adaptively optimization of the ROI window size to improve measurement accuracy and reduce image blur for a vibrating object in order to measure high frequency objects will also be performed.

Acknowledgements

The authors would like to thank the anonymous reviewers for their detailed comments and suggestions which resulted in the improvement of this paper, and Masashi Hashimoto, Tomomi Takashina, and Aoki Hiroshi for their help and support.

References

[1] C. Bräuer-Burchardt, P. Kühmstedt, and G. Notni. Phase error analysis and compensation in fringe projection profilometry. In *SPIE Optical Metrology*, pages 952608–952608. International Society for Optics and Photonics, 2015.

[2] K. Creath. Step height measurement using two-wavelength phase-shifting interferometry. *Applied optics*, 26(14):2810–2816, 1987.

[3] N. D'Apuzzo. Overview of 3d surface digitization technologies in europe. In *Electronic Imaging 2006*, pages 605605–605605. International Society for Optics and Photonics, 2006.

[4] L. Ekstrand and S. Zhang. Autoexposure for three-dimensional shape measurement using a digital-light-processing projector. *Optical Engineering*, 50(12):123603–123603, 2011.

[5] M. Frigo and S. G. Johnson. Fftw: An adaptive software architecture for the fft. In *Acoustics, Speech and Signal Processing, 1998. Proceedings of the 1998 IEEE International Conference on*, volume 3, pages 1381–1384. IEEE, 1998.

[6] J. Geng. Structured-light 3d surface imaging: a tutorial. *Advances in Optics and Photonics*, 3(2):128–160, 2011.

[7] D. C. Ghiglia and M. D. Pritt. *Two-dimensional phase unwrapping: theory, algorithms, and software*, volume 4. Wiley New York:, 1998.

[8] S. S. Gorthi and P. Rastogi. Fringe projection techniques: whither we are? *Optics and lasers in engineering*, 48(IMAC-REVIEW-2009-001):133–140, 2010.

[9] J. Gühring. Dense 3d surface acquisition by structured light using off-the-shelf components. In *Photonics West 2001-Electronic Imaging*, pages 220–231. International Society for Optics and Photonics, 2000.

[10] M. Gupta, A. Agrawal, A. Veeraraghavan, and S. G. Narasimhan. Structured light 3d scanning in the presence of global illumination. In *Computer Vision and Pattern Recognition (CVPR), 2011 IEEE Conference on*, pages 713–720. IEEE, 2011.

[11] S. Heist, M. Sieler, A. Breitbarth, P. Kühmstedt, and G. Notni. High-speed 3d shape measurement using array projection. In *SPIE Optical Metrology 2013*, pages 878815–878815. International Society for Optics and Photonics, 2013.

[12] P. S. Huang, C. Zhang, and F.-P. Chiang. High-speed 3-d shape measurement based on digital fringe projection. *Optical Engineering*, 42(1):163–168, 2003.

[13] M.-S. Jeong and S.-W. Kim. Color grating projection moiré with time-integral fringe capturing for high-speed 3-d imaging. *Optical Engineering*, 41(8):1912–1917, 2002.

[14] Y. Ji. A computer vision-based approach for structural displacement measurement. In *SPIE Smart Structures and Materials+ Nondestructive Evaluation and Health Monitoring*, pages 76473H–76473H. International Society for Optics and Photonics, 2010.

[15] Y. Ji and C. Chang. Nontarget image-based technique for small cable vibration measurement. *Journal of Bridge Engineering*, 2008.

[16] S.-W. Kim and N.-S. Kim. Multi-point displacement response measurement of civil infrastructures using digital image processing. *Procedia Engineering*, 14:195–203, 2011.

[17] C. Liu, A. Torralba, W. T. Freeman, F. Durand, and E. H. Adelson. Motion magnification. *ACM transactions on graphics (TOG)*, 24(3):519–526, 2005.

[18] D. Malacara. *Optical shop testing*, volume 59. John Wiley & Sons, 2007.

[19] D. Moreno, K. Son, and G. Taubin. Embedded phase shifting: Robust phase shifting with embedded signals, 2015.

[20] D. E. Oliver. Scanning laser vibrometer for dynamic deflection shape characterization of aerospace structures. In *SPIE's 1995 Symposium on OE/Aerospace Sensing and Dual Use Photonics*, pages 12–22. International Society for Optics and Photonics, 1995.

[21] G. Sansoni, M. Carocci, and R. Rodella. Three-dimensional vision based on a combination of gray-code and phase-shift light projection: analysis and compensation of the systematic errors. *Applied Optics*, 38(31):6565–6573, 1999.

[22] G. Sansoni and F. Docchio. 3-d optical measurements in the field of cultural heritage: the case of the vittoria alata of brescia. *Instrumentation and Measurement, IEEE Transactions on*, 54(1):359–368, 2005.

[23] T. Weise, B. Leibe, and L. Van Gool. Fast 3d scanning with automatic motion compensation. In *Computer Vision and Pattern Recognition, 2007. CVPR'07. IEEE Conference on*, pages 1–8. IEEE, 2007.

[24] H.-Y. Wu, M. Rubinstein, E. Shih, J. V. Guttag, F. Durand, and W. T. Freeman. Eulerian video magnification for revealing subtle changes in the world. 2012.

[25] Z. Zalevsky, Y. Beiderman, I. Margalit, S. Gingold, M. Teicher, V. Mico, and J. Garcia. Simultaneous remote extraction of multiple speech sources and heart beats from secondary speckles pattern. *Optics express*, 17(24):21566–21580, 2009.

[26] S. Zhang and P. Huang. High-resolution, real-time 3d shape acquisition. In *Computer Vision and Pattern Recognition Workshop, 2004. CVPRW'04. Conference on*, pages 28–28. IEEE, 2004.

[27] S. Zhang, D. Van Der Weide, and J. Oliver. Superfast phase-shifting method for 3-d shape measurement. *Optics express*, 18(9):9684–9689, 2010.

[28] Z. Zhang, C. E. Towers, and D. P. Towers. Time efficient color fringe projection system for 3d shape and color using optimum 3-frequency selection. *Optics express*, 14(14):6444–6455, 2006.

[29] H. Zhao, W. Chen, and Y. Tan. Phase-unwrapping algorithm for the measurement of three-dimensional object shapes. *Applied Optics*, 33(20):4497–4500, 1994.